Applied Catalysis A, General 711 (2026) 120718

Contents lists available at ScienceDirect

Applied Catalysis A, General

journal homepage: www.elsevier.com/locate/apcata

Production of aromatics from furfural and ethanol over zeolite catalysts: Reaction and deactivation mechanisms, effect of acidity and zeolite structures

Francesco Sandri [a], Jennifer Cueto [b], Christoph Schmidt [a], Anssi Peuronen [c], Pia Damlin [c], Teija Tirri [a], Kari Eränen [a], Mika Lastusaari [c], Narendra Kumar [a], David P. Serrano [b,d], Päivi Mäki-Arvela [a], Dmitry Yu. Murzin [a,*]

[a] Laboratory of Industrial Chemistry and Reaction Engineering, Åbo Akademi University, Turku, Åbo 20500, Finland
[b] Thermochemical Processes Unit, IMDEA Energy Institute, Madrid, Móstoles 28935, Spain
[c] Department of Chemistry, University of Turku, Turku 20014, Finland
[d] Chemical and Environmental Engineering Group, Rey Juan Carlos University, Madrid, Móstoles 28933, Spain

ARTICLE INFO

Keywords:
Aromatization
Green BTX
Coke formation
Zeolites
Diels-Alder cyclization
Coke characterization

ABSTRACT

The production of aromatics, specifically benzene, toluene and xylenes (BTX), from bio-derived feedstock such as ethanol and furfural can be achieved by zeolite catalysts. However, the formation of coke strongly limits this reaction leading to catalyst deactivation. In-depth understanding of the relationship between the catalyst characteristics and the mechanism of carbon deposit is needed to improve potential applicability of this novel approach for BTX production. Evaluation of the catalytic activity of β and ZSM-5 zeolites in the aromatization of ethanol and furfural, coupled with the characterization of the spent catalysts, gave important insights on the structure and features that are required to increase the aromatics formation. With these investigations it was possible to determine the location of the catalytic sites that are active in the aromatization reaction, defining at the same time the mechanism of deactivation by coke formation. These findings give important advances for the future design of efficient catalysts for the aromatics production.

1. Introduction

Aromatics are important chemical intermediates and solvents, in particular benzene, toluene and xylenes (BTX), which are currently produced from fossil sources. The annual market size of BTX is ca. 143 million tons in 2025 and is predicted to steadily increase over the years [1]. However, in the frame of a carbon neutral development of the chemical industry, there is a need to shift from non-renewable feedstock to bio-based renewable one. In this context, exploitation of biomass as a raw material for the production of BTX has been highlighted as a promising alternative to obtain platform molecules that can be converted into these higher value chemicals [2,3]. Among several bio-based proposed strategies, the Diels-Alder (DA) condensation of furan and derivatives with a dienophile is gaining more and more importance, due to a possibility to utilize many compounds obtained from processing of lignocellulosic feedstock, such as furan, methylfuran, dimethylfuran, etc., to produce aromatics [4,5]. This strategy involves the reaction between furan or methylated furanic rings, acting as diene, with dienophiles such as light olefins. However, the new approaches for the production of furan relies on a multi-step treatment of biomasses, whereas the commercial production is based on furfural decarbonylation [6]. Moreover, olefins are products of petrochemical industry (i.e. steam cracking of naphtha), although a sustainable production route from biomass derived alcohols by dehydration is practiced industrially [7,8]. Recently a novel approach for the production of green aromatics has been proposed by Gancedo et al. [9], starting from furfural and ethanol. The idea behind this new methodology is to reduce the number of steps needed to obtain aromatics, having in a single catalytic bed decarbonylation of furfural to furan, dehydration of ethanol to ethylene and the DA step leading to aromatics. This ensures a process that starts with compounds directly coming from biomass with a lower number of production steps. The reaction network is displayed Fig. 1. According to the proposed mechanism, benzene would be the only expected product. Nevertheless, the simultaneous presence of benzene, ethylene, and

* Corresponding author.
E-mail address: Dmitry.Murzin@abo.fi (D.Yu. Murzin).

https://doi.org/10.1016/j.apcata.2025.120718
Received 18 September 2025; Received in revised form 14 November 2025; Accepted 24 November 2025
Available online 25 November 2025

Brønsted acid sites enables alkylation and isomerization pathways, thereby leading to formation of a wider spectrum of aromatic compounds [10]. Nevertheless, the mechanism of aromatic formation in the reaction involving olefins and furan-like compounds is still under debate. Another common mechanism proposed in the literature is related to isomerization of furans to unsaturated oxygenated compounds [11], which further react the hydrocarbon pool generated by the olefin [12].

All the reaction steps of the network are catalyzed by acid sites. In the work of Gancedo et al. specifically HZSM-5 zeolite with the SiO_2/Al_2O_3 = 23 was chosen as the catalyst based on a literature survey. The reaction was carried out at 3 bar and 500°C. In that work it was underlined how the combination of ethanol and furfural as the feed brings higher production of BTX and naphthalene as compared to the use of ethylene and furan. Moreover, other studies confirmed an improvement in aromatics production by using furfural instead of furan, when coupled with methanol [13] or single-ring aromatics to obtain naphthalene [14]. Nevertheless, these approaches are still limited by the complete conversion of in-situ generated furan and olefins into BTX, lowering the selectivity of the reaction. Moreover, the catalyst undergoes fouling that causes its deactivation over time strongly limiting its activity. This work investigates the production of biobased aromatics starting from furfural and ethanol, following the aforementioned innovative approach suggested by Gancedo et al. [9]. While the latter work suggested an innovative approach to generate aromatics, no elucidation of the reaction mechanism was given in relation to the catalyst properties and structure, namely presence of Brønsted and Lewis acid sites. Moreover, no correlation between the catalyst properties and deactivation was established, as only one catalyst was tested. In line with the literature, as a starting point in the investigation, HZSM-5 zeolite has been chosen as a catalyst. This catalyst has been already reported to be promising for the aromatization of simple substrates such as light alkanes or furan and methyl-substituted related compounds [4,15]. The main features defining their catalytic activity in the aromatization reactions are the concentration of acid sites and their nature, namely Brønsted (BAS) rather than Lewis (LAS) acid sites. The former can be tuned by changing the SiO_2/Al_2O_3 ratio, whereas the latter can be modified by introducing metals to the zeolite and by tuning the catalytic sites from Brønsted to Lewis ones [16–18]. Specifically, the SiO_2/Al_2O_3 ratio defines density, strength, and distribution of acid sites, affecting reaction pathways, selectivity, and catalyst deactivation. Therefore, an appropriate balance in the SiO_2/Al_2O_3 ratio must be established to optimize catalyst performance. In this work, the focus is on the effect of the SiO_2/Al_2O_3 ratio, while the investigation of metal-doped zeolites was outside of the scope and will be explored separately. Accordingly, several ZSM-5 catalysts with different SiO_2/Al_2O_3 ratios were characterized with different techniques including nitrogen physisorption, pyridine adsorption and ICP-OES, to define their features such as textural properties, concentration and strength of the acid sites and chemical composition. These catalysts were studied subsequently in the aromatization of furfural and ethanol. The characteristic and location of the carbon deposit on the spent catalyst was investigated, achieving a detailed knowledge of the deactivation phenomenon. Moreover, a Hβ zeolite was included in the study, to shade a light on the effect of the zeolite structure in the aromatization reaction.

2. Experimental section

2.1. Materials

The zeolites used in this work have been purchased in the ammonium form from Zeolyst International and turned into the acidic form by calcination at 550°C in a muffle oven. The product numbers for the different SiO_2/Al_2O_3 ratio were as follows; 23: CBV 2314, 50: CBV 5524 G, 80: CBV 8014, 280: CBV 28014. As for the calcination, the target temperature was reached in 290 min with a heating ramp of 1.8 °C/min, and then holding for 720 min. The catalyst was pelletized, ground and sieved. Unless specified, the fraction used for a catalytic experiment is in the range 150–180 μm.

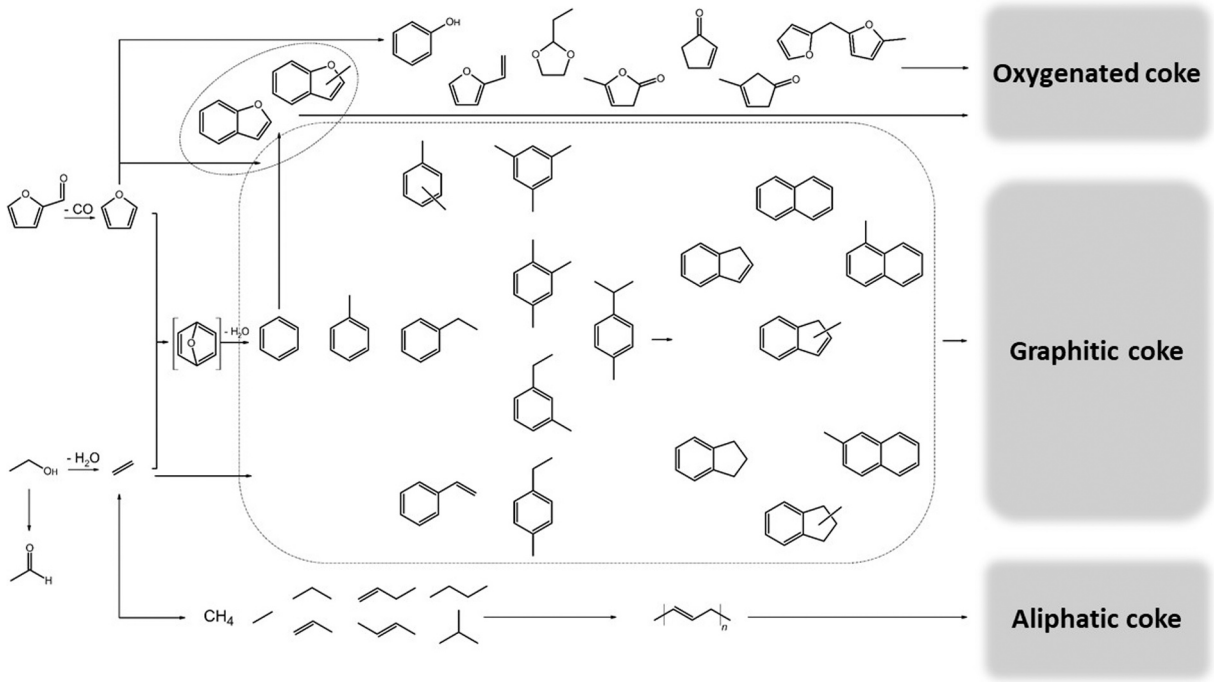

Fig. 1. Reaction scheme for, the production of aromatics from furfural and ethanol, based on the reaction network proposed by Gancedo et al. [9], and implemented with the main compounds found within our investigation.

2.2. Catalysts characterization

The catalysts were analyzed with N_2-physisorption to evaluate the textural properties, with a Micromeritics MicroActive 3Flex 3500 instrument, after an ex-situ under vacuum pretreatment at 180°C for 24 h. The total surface area was calculated with the Dubinin-Radushkevich model, the pore volume is calculated from the DFT model assuming a cylindrical shape of the pores, and the external surface area, namely the area of the external surface of the catalysts grains, was calculated from the t-plot. Thermogravimetric analysis (TGA) of the spent catalysts was performed with a TA Instrument SDT650, using a 10 °C/min heating ramp up to 800°C, under air atmosphere (50 mL/min). Brønsted and Lewis acid sites characterization was performed by FT-IR using pyridine as the probe molecule. The samples were pressed to form a disc, which was inserted on a cell with ZnSe windows. The sample was pretreated at 450°C under vacuum ($8{\cdot}10^{-3}$ bar) for three hours and exposed to pyridine vapors. The pyridine treatment was performed flowing N_2 (5 mL/min) at atmospheric pressure through liquid pyridine, mixing the pyridine flow with 35 mL/min N_2 flow and sending the total flow to the sample for 30 min while keeping it at 100°C. The catalyst was treated with different temperature steps (150°C, 250°C, 350°C and 450°C), where a part of the pyridine desorbs, and cooled down at 100°C in between each step. After each thermal treatment, the IR spectra of the sample were recorded with a Shimadzu IRTracer-100 FT-IR operating in transmittance mode, while the sample was at 100°C. The IR signal was correlated to the concentration of adsorbed pyridine, and therefore to the concentration of acid sites. Pyridine bound to the Brønsted acid sites gives a signal at 1515–1565 cm^{-1}, whereas the one absorbed on the Lewis acid sites exhibits a signal in the range 1435–1470 cm^{-1}. Taking into account the molar extinction coefficient from the reference [19], the concentration of acid sites can be calculated, using the spectra of the catalyst after the pretreatment at 450°C as the background. Raman measurements were performed using a Renishaw inVia confocal Raman microscope (Leica). A 532 nm laser was employed for excitation, with laser power intensities ranging from 1 % to 100 %, depending on the sample sensitivity. Raman spectra were acquired using either a 50X or 100X objective lens unless otherwise stated. The Raman-scattered light was dispersed using an 1800 lines/mm diffraction grating and detected with a Peltier-cooled charge-coupled device (CCD) detector. Spectra were collected over a range of 125–3200 cm^{-1} or 125–1600 cm^{-1} to cover characteristic vibrational modes of the catalyst and spent catalyst materials. The spectrometer was calibrated using a silicon standard with a reference peak at 520.5 cm^{-1}. XRD powder patterns were collected using PANalytical Aeris powder X-ray diffractometer equipped with PIXcel1D-Medipix3 detector by using Cu-Kα1,α2 radiation (λ = 1.5406 Å, 1.5444 Å). The samples were prepared on a Si zero-background sample holder and data were recorded in the 2θ-range of 5–60° using step size of 0.02° and counting time of 89 s per step. XRD patterns were analyzed using the HighScore software suite [20] and the reference patterns were acquired from the ICDD PDF-4 + database [21]. ICP-OES analyses were performed using a PerkinElmer Optima 7300 DV instrument. The catalysts were digested prior to analysis in an Anton Paar MW3000 microwave system with a 2:1 volumetric mixture of nitric and hydrofluoric acids. Calibration was performed with standard solutions of known aluminum concentrations.

2.3. Catalytic experiment

In the catalytic experiments, ethanol (VWR Chemicals, 99.93 %) was used as such, whereas furfural (Sigma-Aldrich, 99 %) was previously distilled under vacuum, to avoid contamination by products of furfural degradation, mainly humins, and ensure a better reproducibility of catalytic experiments. To distill furfural, the liquid was placed in a round-bottom flask and heated at 68°C, while the system was connected to a Vigreux column followed by a condenser and a receiving flask, using a water pump to apply the vacuum to the line. The purity of the distillate was ensured with a GC-FID analysis. The reactor set-up consisted of a 4 mm stainless steel tubular reactor heated by a furnace, where the catalytic bed was placed and separated by the inert filling material (glass beads) with two quartz wool layers. The catalytic bed was composed of 1 g of catalyst, diluted with 0.2 g of glass beads. The furnace was heated to 300–500°C depending on the experiment, whereas no pressure controller was used, to have the system operating at ambient pressure. During the catalytic experiments the pressure is monitored to detect any possible pressure increase due to pressure drops. The reactants were fed with two syringe pumps (Chemyx Fusion 6000X), using a liquid flow of 0.0293 mL/min of ethanol and 0.0207 mL/min of furfural, unless differently specified. Helium (Woikoski, 99.996 %), used as an inert gas to tune the residence time of the reactant, was fed to the system with a mass flow controller (Brooks 58505) at a flow rate of 50 mL/min. With this configuration, the total flow of the reactant is 0.0500 mL/min, with a molar ratio of furfural/ethanol = 1:2, and a WHSV = 2.83 h^{-1}. The reactor was connected to a gas/liquid separator, which cools the gas flow to 1°C and allows separation of the liquid phase from the gas stream. The liquid phase, typically a biphasic solution, was entirely removed from the collecting flask in each sampling and analyzed with a gas-chromatograph (Agilent Technologies 6890 N) equipped with a DB-5 column (Agilent 123–506E) and a FID detector. Prior to the analysis, the liquid sample was diluted with a known volume of a 5 g/L cyclohexanol (J. T. Baker, ≥99 %) in 1,4-dioxane (Honeywell, ≥99.0 %). This has the double function to homogenize the biphasic solution, ensuring the reliability of the analysis, and to add cyclohexanol as the internal standard. More information about the GC analysis are reported in SI1 section. To identify the products in the liquid phase, the samples were also analyzed with an Agilent 6890 GC/MS equipped with a 5973 Network Mass Selective Detector, by using the same column and the method utilized with the gas-chromatograph equipped with the FID detector. Moreover, the as prepared sample solution was analyzed with the Karl-Fischer titration to determine the water content, using a 736 GP Titrino and Honeywell HYDRANAL™ Composite 2 as the titrant. The gas composition was determined with an Agilent 3000 A microGC equipped with three columns (Molecular sieve, Plot Q and OV-1). To quantify the yield of the products in the gas phase, the chromatographic analysis was coupled with the measurement of the total volume of the gas produced, using a drum-type gas meter (Ritter TG 0.5/5). The yield of each component can be calculated by the total volume of the outgoing gas and its concentration, derived from microGC analysis. More information about the micro-GC analysis is reported in SI1 section. The carbon mass balance was calculated according to the following equation:

$$\%_{C_i} = \frac{mol_i \cdot n_{C_i}}{\sum 5 \cdot mol_{FFL,in} \cdot 2 \cdot mmol_{EtOH,in}} \cdot 100$$

With $\%_{C_i}$ the percentage of carbon atoms of a given compound having n_{C_i} carbon atoms, and mol_i its yield in mol quantified in a given TOS range. $mol_{FFL,in}$ and $mmol_{EtOH,in}$ the moles of furfural and ethanol fed to the reactor in that given TOS range.

3. Results and discussion

3.1. Catalysts characterization

Chemical and physical properties of the catalysts investigated are presented in Table 1.

From the structural characterizations it can be noticed that the average pore size calculated with the DFT model is in good agreement with the expected value for the MFI structure [9,23]. The surface area as well as the pore volume are rather constant as the aluminum content changes. Moreover, the characterization of the acid sites by pyridine adsorption is reported in Fig. 2. More information on the results of the analysis is reported in SI2 section. Because of the above acid sites characterization results, it is possible to define a trend for the

Table 1
Textural properties and SiO_2/Al_2O_3 ratios of the HZSM-5 and Hβ zeolite catalysts.

Zeolite	Nominal SiO_2/Al_2O_3	Calculated SiO_2/Al_2O_3	Surface area [m^2/g]	External surface area [m^2/g]	Total pore volume [cm^3/g]	Micropores volume [cm^3/g]	Average pore size of micropores [nm]
HZSM-5	23	26.4	426	69	0.22	0.21	0.59
HZSM-5	50	67.9	462	143	0.25	0.22	0.59
HZSM-5	80	100.4	489	155	0.28	0.23	0.59
HZSM-5	280	343.7	458	162	0.26	0.21	0.59
Hβ	38	22 [22]	757	155	0.39	0.32	0.63

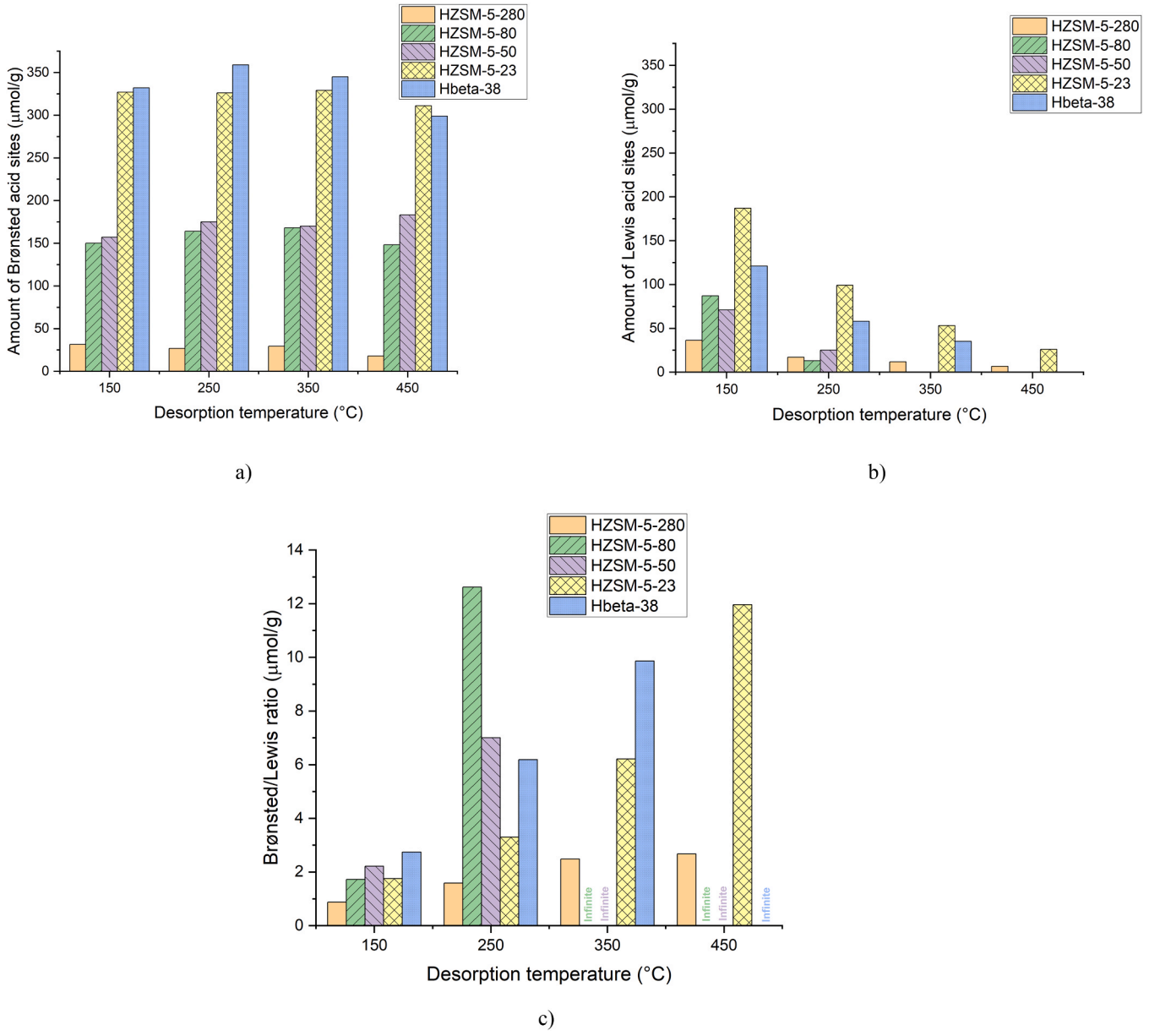

Fig. 2. Acid sites distribution in the zeolites, calculated from IR analysis of the adsorbed pyridine. On the left panel the Brønsted acid sites are reported, while on the right panel the Lewis acid sites are presented, both as a function of the pyridine desorption temperature. In the lower panel the ratio of Brønsted over Lewis acid sites is reported as a function of the pyridine desorption temperature.

concentration, strength and nature of acid sites depending on the SiO_2/Al_2O_3 ratios of ZSM-5 zeolites.

As for the acid sites, the concentration of BAS detected at any temperature is constant for all the zeolites, meaning that all the BAS present in the materials were very strong and able to interact with pyridine at temperature as high as 450°C. The HZSM-5–23 has a double concentration of BAS when compared to the other two HZSM-5 zeolites, as expected from its higher aluminum content. As to the LAS, the HZSM-5–23 and Hβ-38 zeolites have a higher content of those, when compared with the two other HZSM-5 materials. The higher content of LAS is related to the presence of extra-framework aluminum species [24], which is typically much higher in the case of the Hβ zeolite [25]. In more detail, at 150°C, the concentration of LAS was determined to be 336 µmol/g for Hβ38 and 187 µmol/g for HZSM-5–23. In contrast,

HZSM-5–50 and HZSM-5–80 exhibited LAS concentrations below 100 μmol/g, with no detectable LAS remaining after desorption at 350°C. HZSM-5–280 displayed only negligible acidity, in agreement with its low aluminum content.

3.2. Catalytic results

3.2.1. Preliminary results

A preliminary screening of the HZSM-5 catalyst has been done by loading in the reactor 300 mg of the catalyst, while keeping all the other experimental parameters as described in the experimental section, therefore achieving a WHSV of 11.3 h^{-1}. The total flow rate of the reactant was set to be 0.751 mmol/min, with a molar ratio of furfural to ethanol equal to 1:2. This molar ratio was selected to have a double fraction of ethanol with respect to furfural, as it can be expected that the main reasons related to the catalyst deactivation are related to the presence of furfural. However, under these conditions fast catalyst deactivation was observed, and no aromatics were obtained. As expected, deactivation was due to formation of a carbon deposit that blocks the catalytic sites. This was directly visible by color changes in the spent catalyst, which turned black after the reaction. Another highlight coming from the preliminary investigation was that the lower was the SiO_2/Al_2O_3 ratio, the stronger was catalyst deactivation (Fig. SI3). Consequently, the catalyst loading was increased up to 1 g, with a subsequent decrease of WHSV to 2.8 h^{-1}. These conditions are more similar to those already reported in the literature by Gancedo et al. [9], where in that case the WHSV is 2.1 h^{-1}. The most promising catalyst in the preliminary investigations was HZSM-5 zeolite with the SiO_2/Al_2O_3 ratio of 80, in terms of resistance towards deactivation. For this reason, this catalyst was chosen to be tested under low WHSV (2.8 h^{-1}) conditions and with WHSV 2.1 h^{-1} and equimolar flow of ethanol and furfural to compare the results with those reported in the literature. Moreover, a blank experiment feeding the reactants with the ratio ethanol/furfural: 2/1 with the same flow rates used in the experiment at WHSV = 2.8 h^{-1} has been performed, not resulting in the transformations of any reactant.

The carbon mass balance of the two experiments using the HZSM-5–80 with different WHSV and different composition of the feed is presented in Fig. 3. Before describing the specific results, it is important to give an overview of the products, underlining a very broad product distribution. The first classification of the reaction product can be done depending on the phase where the compounds were observed. In the gas phase mainly CO was present, coming from the decarbonylation of furfural, as well as ethylene, the product of ethanol dehydration. Moreover, other compounds were present in the gas phase (Fig. SI4c), such as CO_2, derived from degradation of furan [26], methane, saturated and unsaturated hydrocarbons with carbon atoms between two and four. The liquid phase was composed mainly of water, with its content ranging from ca. 50–65 % in the beginning of the reaction (TOS = 80 min) up to > 95 % at a longer reaction time (Fig. SI4a). Typically, a decrease in the water content was observed in the last sampling at TOS = 320 min, and in general the trend of water production was very similar for both experiments reported in Fig. 3. The liquid phase contained also a separate organic phase, which was composed mainly of aromatic compounds. Among those, the most abundant ones were benzene, toluene and xylenes. Moreover, many other single-ring aromatics were present, such as ethylbenzene, pseudocumene, mesitylene and p-cymene. In addition, multi-ring aromatics were found, such as indene, naphthalene and methyl-substituted related compounds. These compounds are reported in the red bar of Fig. 3. Some other compounds were present in the liquid phase in lower fractions, such as acetaldehyde, acetone, and benzofuran. It is worth underlining that many volatile compounds were present in both phases. This was the case of furan (blue bar), with > 99 % found in the gas phase. Despite the cooling system designed to separate the liquid and the gas phase, benzene and toluene were almost totally present in the gas phase. In more detail, the yield of benzene in the liquid phase never exceeded 5 % of the total production while for toluene the highest content was 25 % of its total yield. Because of this incomplete condensation, only maximum 10 % of the total carbon of the products was found in the liquid phase. Finally, it is worth emphasizing that many other compounds were detected in the liquid phase by GC-MS analysis, however they could not be quantified as the standards for the calibration are not available. Conversely, these substances were present in very small yield, estimated to be overall below 3 mol% of the total yield of organic compounds present in the liquid phase. Among these compounds, the most relevant are styrene, 3-ethyltoluene, 4-ethyltoluene, phenol and indane. Since they cannot be quantified, these compounds are not included in the carbon mass balance. However, they are present in small yield, therefore the carbon missing in the mass balance is due mainly to the formation of carbon deposits on the catalyst.

As for the experiments reported in Fig. 3, only few differences can be noticed coming from different compositions of the feed. As the relative fraction of furfural present in the experiment with WHSV = 2.1 h^{-1} was higher, a higher yield of furan and CO, together with a lower yield of ethylene in the products were obtained. Moreover, in both experiments a total conversion of both reactants was achieved for TOS ≤ 260 min. Another difference between the two experiments consists of the production of aromatics, which can be partially noticed from the carbon mass balance in Fig. 3. As the yield of aromatics in the mass balance is

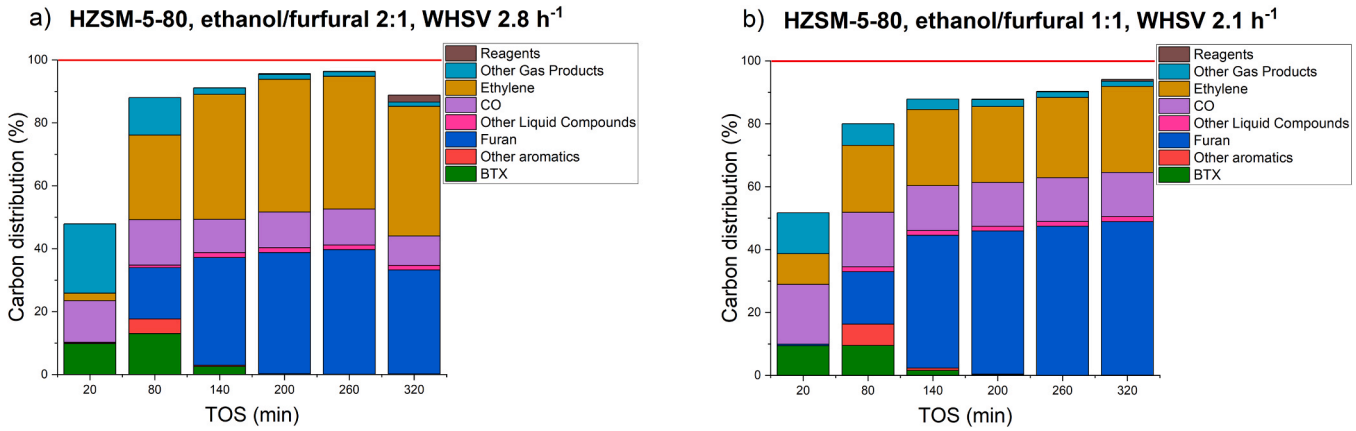

Fig. 3. Carbon mass balance of the experiments with HZSM-5–80 at 500°C. a) results with WHSV = 2.8 h^{-1} and a molar flow with ratio ethanol/furfural 2:1. b) results with WHSV = 2.1 h^{-1} and a molar flow with ratio ethanol/furfural 1:1. "Reagents" includes unreacted ethanol and furfural. "Other gas products" includes CO_2, CH_4, C_2H_6, C_3H_6, C_4H_8, i-C_4H_{10} and n-C_4H_{10}. "Other liquid compounds" includes acetaldehyde, acetone and benzofuran. "Other aromatics" includes ethylbenzene, cumene, mesitylene, pseudocumene, p-cymene, indene, naphthalene, 1-methylnaphthalene and 2-methylnaphthalene.

low when compared to other compounds, the production of aromatics over TOS is reported in details in Fig. 4, to better visualize the differences, together with the selectivity towards different classes of aromatics.

In these investigations of the catalytic activity of the HZSM-5–80 zeolite an important aspect regarding the catalyst deactivation can be pointed out. In fact, the catalyst afforded complete conversion of the reactants in the initial steps of the reaction network, i.e. decarbonylation of furfural to furan and dehydration of ethanol to ethylene. On the other hand, the catalyst deactivated in the following steps of the reaction network, i.e. those related to the production of aromatics. In terms of aromatics production, deactivation is already visible at TOS $\geq$ 80 min giving completely inactive catalyst at TOS $\geq$ 260 min. At TOS = 20 min, 50 % of carbon balance is missing. This can be partially attributed to the system dynamics at the beginning of the experiment and also to formation of carbon deposits over the catalyst at the very beginning of the reaction. Coke is gradually formed because of aromatics production blocking the catalytic sites. To better define the reason for deactivation, catalytic experiments with the single reactants were performed. For the following catalytic experiments, it was decided to operate with the higher WHSV (2.8 h^{-1}), and with a ratio ethanol/furfural of 2:1. The reason is that under such conditions selectivity towards aromatics is higher. This, coupled with a higher WHSV, gives a better understanding of the mechanism of aromatics formation. Prior to mechanistic and deactivation studies it was important to exclude the presence of mass transfer limitation. Therefore, once defined the reaction conditions, in terms of WHSV and the ratio of the reactants, the zeolite HZMS-5 80 has been studied in the reaction, by using different grain sizes of the catalyst, namely 90–150 μm, 150–180 μm, and 180–250 μm, respectively. The results, reported in Fig. SI5, display only small differences between different fractions, that can be attributed only to experimental errors. Therefore, it can be concluded that the catalytic performance under these conditions is not affected by intragrain mass transfer limitations. Finally, the performance of the Hβ-38 zeolite was studied, to investigate the effect of the zeolite structure in the aromatization reaction. However, the catalyst exhibited a very limited aromatic production, being less than 3 % of the carbon converted in BTX. On the other hand, the catalyst underwent very strong deactivation due to coke formation. This phenomenon was so extensive that the reactor was almost completely clogged, resulting in a pressure increase up to 15 bar which forced the experiment to be stopped at TOS = 240 min. For this reason, it was decided not to continue any further investigations with the Hβ zeolites.

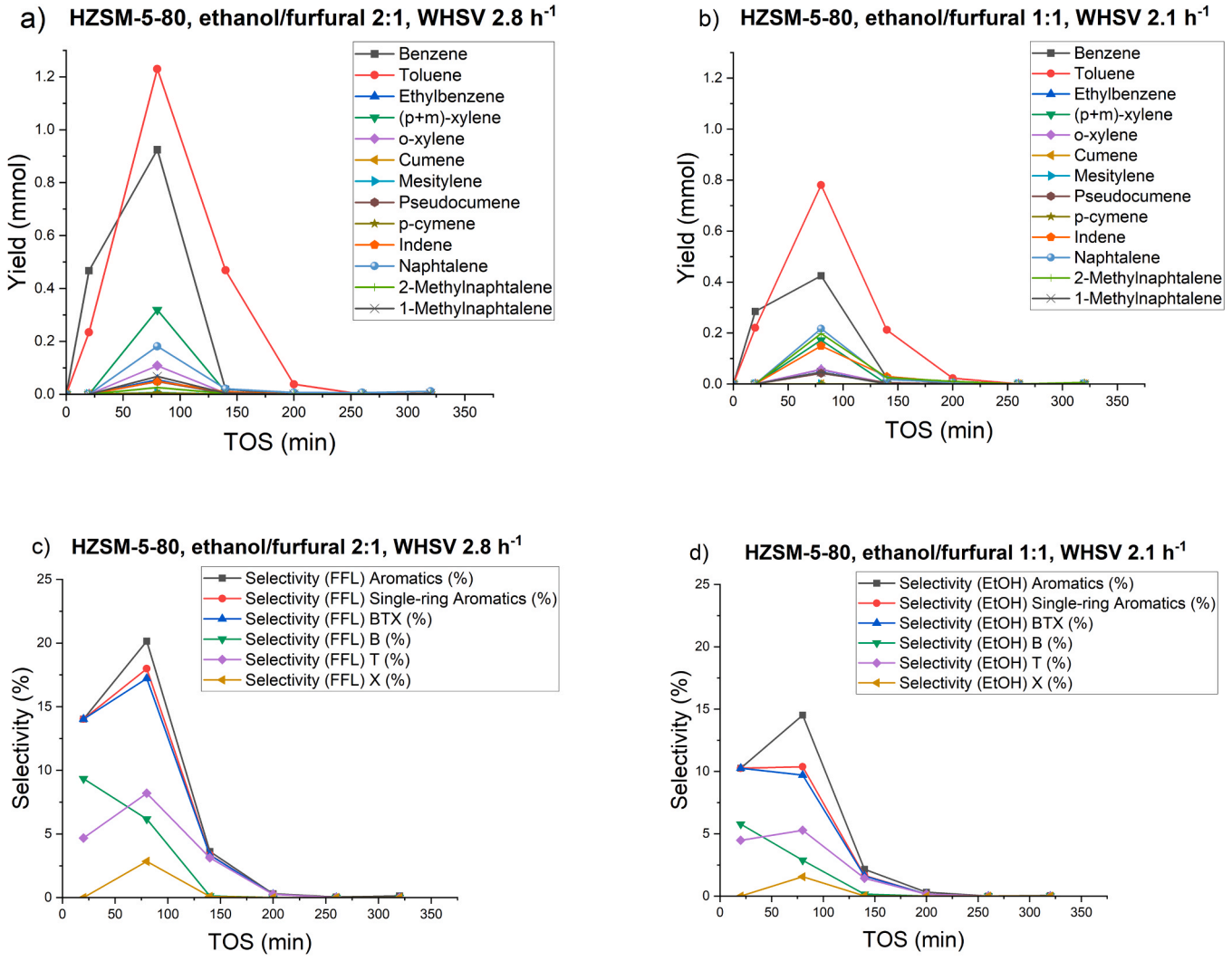

Fig. 4. Aromatic production and selectivity towards aromatics as a function of time, for the experiments with HZSM-5–80. a) aromatic production with WHSV = 2.8 h^{-1} and a molar flow with ratio ethanol/furfural 2:1. b) aromatic production with WHSV = 2.1 h^{-1} and a molar flow with ratio ethanol/furfural: 1/1. c) selectivity with WHSV = 2.8 h^{-1} and a molar flow with ratio ethanol/furfural 2:1. d) selectivity with WHSV = 2.1 h^{-1} and a molar flow with ratio ethanol/furfural 1:1.

3.2.2. Effect of feedstock

The HZSM-5–80 catalyst was studied in the reaction with a single reactant to shade light on the mechanism of the aromatics formation and deactivation. The WHSV was kept the same as in the previous experiment (2.8 h^{-1}), meaning that the volumetric flow was set at 0.0622 mL/min and 0.0438 mL/min for furfural and ethanol, respectively. The results of the experiments are reported on Fig. 5, where the carbon mass balance is shown.

These experiments clearly show that furfural alone yields only traces of aromatics, consisting mainly of BTX at TOS = 20 min and bicyclic aromatics at TOS = 80 min. Moreover, deactivation starts to be visible at TOS = 260 min and at the end of the reaction the conversion dropped to 37 %. On the other hand, by feeding pure ethanol, the production of aromatics was considerably higher and more constant over time. In fact, 23 % of carbon formed BTX at TOS = 140 min, whereas at TOS = 320 min the values decreased only to 18 % (Fig. 5). This result outperformed also the data obtained with the mixture of the reactant (Fig. 3), where the maximum fraction of carbon transformed to aromatics was 13 % at TOS = 80 min. The carbon missing in the balance with the experiment using pure ethanol was not due to carbon formation, but to the formation of gaseous compounds that were not calibrated and thus quantified. Those are most likely saturated and unsaturated hydrocarbons with 3–5 carbon atoms. The yield of acetaldehyde was higher than in the experiments with the mixture of reactants, as 4.5 % of the carbon is found in that compound. Therefore, aldehydes with a higher number of carbon atoms could be included in the unquantified compounds as well. Lower amounts of carbon deposits explain a lower extent of deactivation, and this was confirmed by characterization of the spent catalysts, which will be discussed below. In general, it can be proposed that furfural is mainly responsible for catalyst deactivation, which is in line with the experiments conducted for the mixture of the reactants. However, when ethanol was present in the reaction together with furfural, deactivation originated from furfural transformation was partially inhibited which could be explained by the presence of a dienophile, i. e. ethylene, that converts a part of the furan formed and prevents catalyst deactivation. The best conditions to produce aromatics appeared to be achieved when only neat ethanol was involved in the reaction (Fig. 5), in agreement with the literature on production of aromatics from alcohols [27–30]. In line with the reaction network in Fig. 1, the production of aromatics from alcohols occurs through a primary dehydration step followed by the cyclization of the olefins with a mechanism that differs from the DA mechanism achieved in the presence of a diene. On the other hand, this investigation shows how the production of aromatics from furfural, hardly reached due to deactivation, can be achieved by adding ethanol to the reaction mixture, unlocking a new reaction pathway that enables the transformation of furfural to BTX.

3.2.3. Effect of temperature

To better investigate the reaction mechanism, avoiding excessive catalyst deactivation, experiments at a lower temperature were performed, using the mixture furfural/ethanol in the ratio 1:2 (Fig. SI6a and Fig. SI6b). In particular, the reaction was investigated at 300°C and 400°C. The former case resulted in a very low conversion of furfural and ethanol not giving aromatics. The liquid phase, that typically was a biphasic mixture composed mainly by water, in this case was a single phase containing mainly ethanol and furfural. In the first liquid sample (TOS = 80 min) some small peaks were detected in the GC analysis. Based on GC-MS analysis, these were attributed to products of furfural rearrangement which concentration steadily decreased with TOS. In the gas phase only a small amount of CO (at the beginning of the experiment), furan and hydrocarbons were present (see Fig. SI6a). As for the experiment at 400°C, in the liquid phase small traces of aromatics were detected in the first liquid sample (TOS = 80 min). In the same sample, acetic acid, benzofuran and many heavy compounds of furfural rearrangement were present. At higher TOS no compounds were observed, besides the reactants. Even if a small fraction of ethanol and furfural were still converted with the conversion steadily decreasing with TOS. Such low, but non negligible activity, can be seen from the gas phase analysis showing the presence of ethylene, CO and furan. Interestingly, furan was present in a lower yield when compared to CO, probably giving carbon deposits (see Fig. SI6b). Considering the reaction network in Fig. 1, a temperature lower than 500°C leaves locked the aromatics formation with the DA mechanism, leading to generation of oxygenated compounds that are eventually forming an oxygen-rich carbon deposit. Another important highlight of these experiments is that not only for aromatics, but in general formation of products in the reaction network is strongly inhibited below 500°C. In particular, decarbonylation of furfural and dehydration of ethanol were not taking place. This is an interesting outcome, as the ethanol dehydration is well known to occur below 500°C [31,32]. The origin of complete catalyst deactivation can be attributed to the presence of furfural, although the deactivation mechanism is probably different compared to the one occurring at 500°C, as the products of furfural rearrangement are not detected in that case. At a lower temperature decarbonylation of furfural on the one hand is less efficient, and on the other hand the temperature is not high enough to avoid formation of the oxygenated coke [33]. Therefore, it can be concluded that below 500°C the catalyst is almost totally

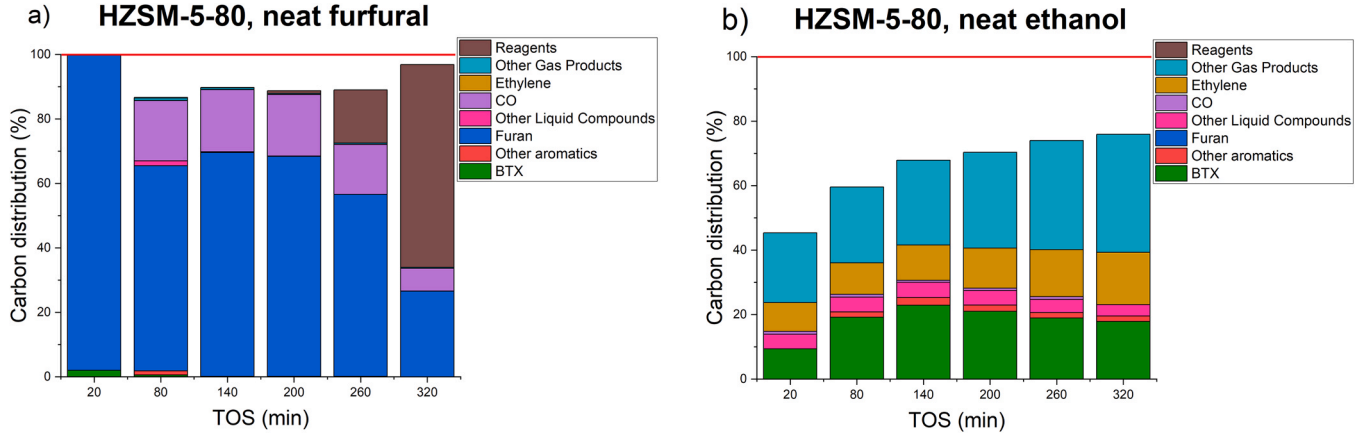

Fig. 5. Carbon mass balance and selectivity of the experiments with HZSM-5–80 at 500°C. a) results of the carbon mass balance feeding only ethanol and b) results of the carbon mass balance feeding only furfural. Both experiments have WHSV= 2.8 h^{-1}. "Reagents" are the reagents used in the reaction, namely ethanol and furfural. "Other gas products" includes CO_2, CH_4, C_2H_6, C_3H_6, C_4H_8, i-C_4H_{10} and n-C_4H_{10}. "Other liquid compounds" includes acetaldehyde, acetone and benzofuran. "Other aromatics" includes ethylbenzene, cumene, mesitylene, pseudocumene, p-cymene, indene, naphthalene, 1-methylnaphthalene and 2-methylnaphthalene.

deactivated due to formation of the oxygenated coke, whereas above 500°C mainly graphitic coke is formed (see Section 3.3). However, this carbon deposit takes longer time to be formed, allowing aromatics production at the beginning of the reaction. A further experiment was carried out to confirm this hypothesis, by running the reaction using neat ethanol at 400°C. In this case, the catalyst was active in dehydration of ethanol and formation of aromatics, with complete conversion of ethanol (see Fig. SI7). In this experiment, the catalyst is less active in the production of aromatics, when compared to the experiment at 500°C, due to slower kinetics of aromatic formation. On the other hand, conversely from the experiment at 500°C, the production of aromatics slightly increased over time. In the same way as for the aromatics production, the kinetics of coke formation is enhanced by a higher temperature, leading to faster catalyst deactivation.

3.2.4. *Effect of the SiO_2/Al_2O_3 ratio*

The effect of the concentration of acid sites was studied for the production of aromatics with the mixture of furfural and ethanol. For this purpose, four different zeolites with different nominal values of SiO_2/Al_2O_3 ratios, namely 23, 50, 80 and 280 were studied. The calculated SiO_2/Al_2O_3 values are slightly different as reported in Table 1. All the catalysts were tested at 500°C, keeping the WHSV = 2.8 h^{-1}. Results of the catalytic experiments with the catalysts HZSM-5–23, HZSM-5–50, HZSM-5–280 are reported in Fig. 6, where they are compared with the previous results obtained with HZSM-5–80.

Fig. 7 gives an overview of the sum of the aromatics produced for each of the catalysts investigated up to TOS = 320 min.

The performance of HZSM-50, HZSM-5–80 and HZSM-5–280 catalysts was rather similar regarding the decarbonylation and dehydration reactions, since they proceed until the end of the catalytic experiments, with only minor deactivation of HZMS-5–80 being observed at TOS = 320 min. This corresponds to a decrease of furfural conversion down to 97 % and a decrease of ethanol conversion to 99 %. Moreover, HZSM-5–50 and HZSM-5–280 catalysts still showed a total conversion of both reactants at the end of the reaction. On the other hand, the HZSM-5–23 catalyst strongly deactivated for all reactions of the reaction network, as reported in Fig. 8. This catalyst has a higher acidity when compared to two other investigated catalysts (Fig. 2), either for Brønsted or Lewis acid sites. On the other hand, the production of aromatics stops for all the catalysts after TOS exceeding 140 min.

As for the BTX production, the HZSM-5–80 catalyst demonstrated a higher production of benzene and toluene when compared to the other zeolites, but was somewhat outperformed by HZMS-5–50 catalyst in the production of xylenes (Fig. 7). Formation of benzene was the same for HZSM-5–23 and HZSM-5–50, whereas in the toluene production HZSM-5–50 zeolite exhibited performance in between HZSM-5–23 and HZSM-5–80 catalysts. On the other hand, HZSM-5–50 gave a higher production of multi-ring aromatics when compared to the other three catalysts, because it generates 0.786 mmol against 0.400 mmol, 0.393 mmol and 0.435 mmol by HZSM-5 23, HZSM-5 80 and HZSM-5–280 catalysts respectively. Finally, the HZSM-5–280 catalyst exhibits a very low aromatic production, in particular BTX, coming from the very low concentration of acid sites, even though their concentration was still enough to ensure a total conversion of both reactants at any TOS. Interestingly,

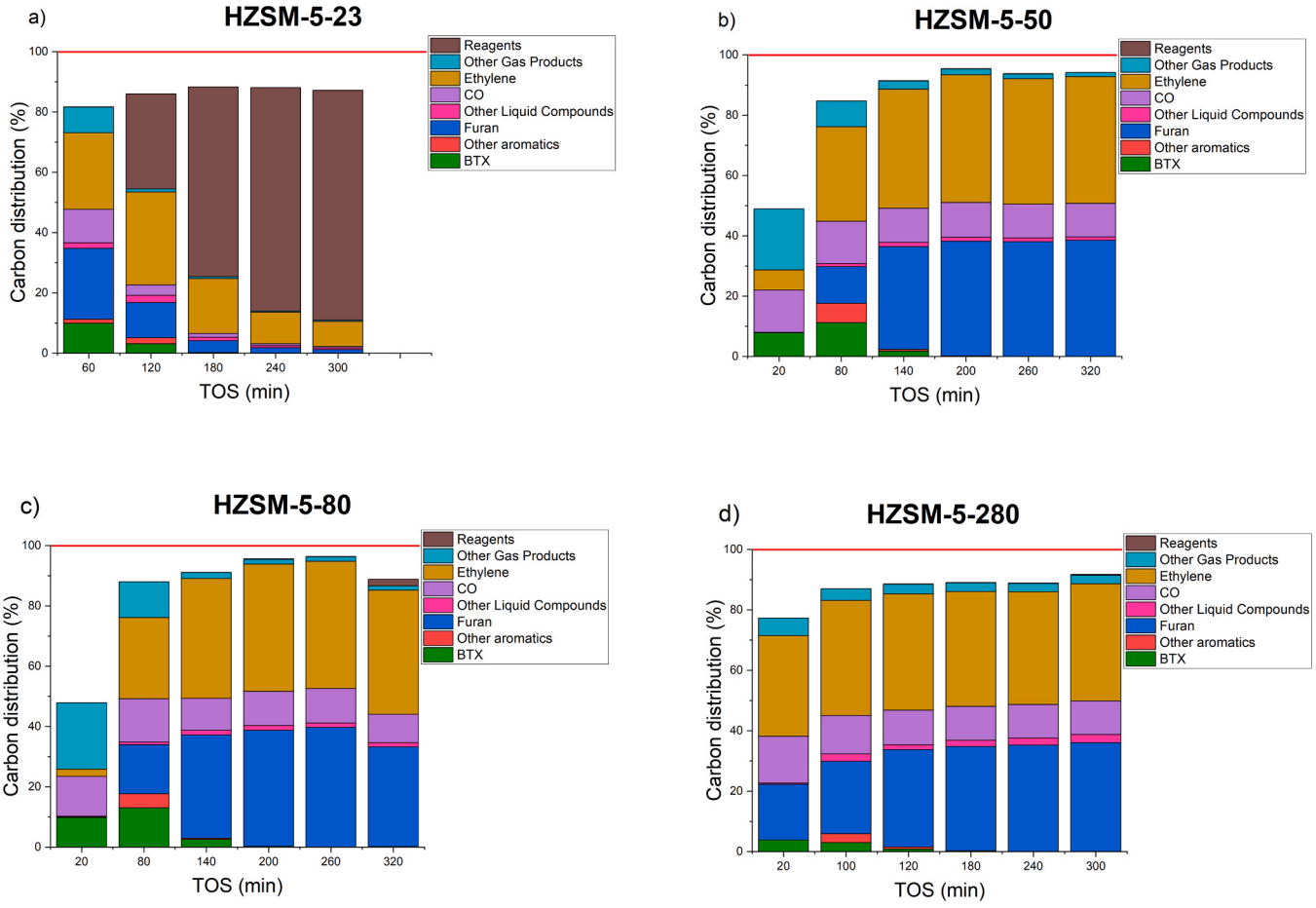

Fig. 6. Carbon mass balance of the experiments with HZSM-5 at different SiO_2/Al_2O_3 ratios at 500°C. a) 23, b) 50, c) 80, d) 280. All experiments have a feed of ethanol/furfural 2:1, with WHSV= 2.8 h^{-1}. "Reagents" includes unreacted ethanol and furfural. "Other gas products" includes CO_2, CH_4, C_2H_6, C_3H_6, C_4H_8, i-C_4H_{10} and n-C_4H_{10}. "Other liquid compounds" includes acetaldehyde, acetone and benzofuran. "Other aromatics" includes ethylbenzene, cumene, mesitylene, pseudocumene, p-cymene, indene, naphthalene, 1-methylnaphthalene and 2-methylnaphthalene.

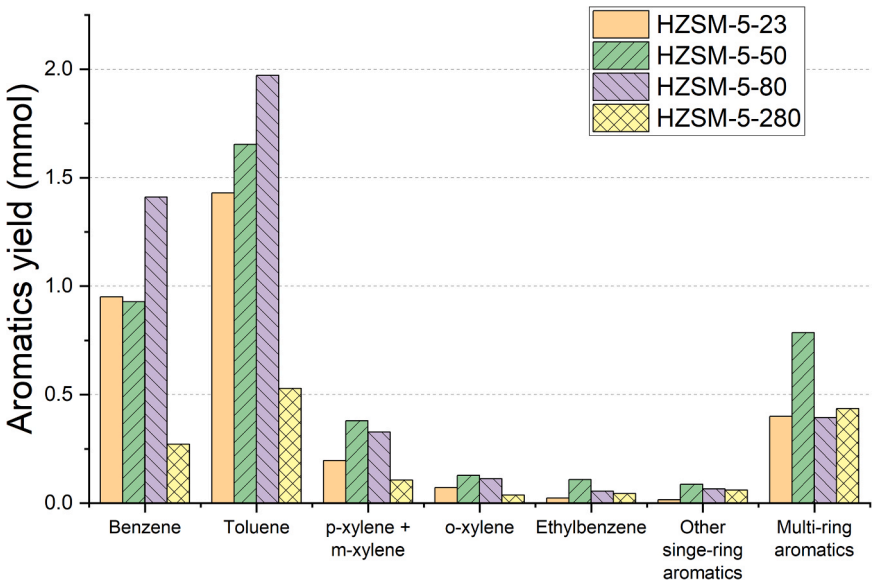

Fig. 7. Product distribution of aromatic compounds using HZSM-5 zeolites with different SiO_2/Al_2O_3 ratios.

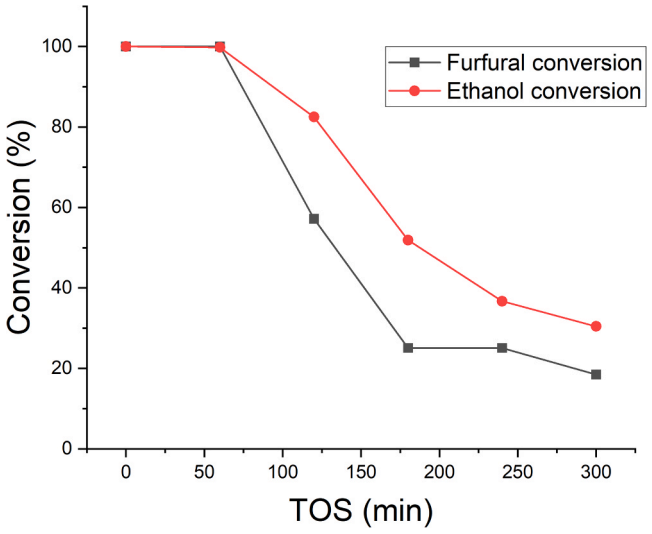

Fig. 8. Conversion of furfural and ethanol for HZSM-5–23 catalyst as a function of TOS, at 500°C, with a feed of ethanol/furfural 2:1 and WHSV= 2.8 h^{-1}.

the yield of multi-ring aromatics equals to those produced by the other catalysts, excluding HZSM-5–50. However, deeper understanding of the catalytic activity can be achieved by looking at the yield of aromatics formed per catalytic site. This value can be seen as the turnover number of the catalyst, typically used to define the activity of a catalytic site before its deactivation. In this case, it represents a better parameter than the turnover frequency, as the strong deactivation noticeably changes the activity over time, making this parameter less useful to define the properties of the catalysts. In Fig. 9 the activity of the single catalytic sites as a function of either the total BAS or LAS concentration (on panel a) and b), respectively) is displayed. Theoretically these values can be assumed to be equal to the concentration of BAS or LAS detected by pyridine adsorption at T = 150°C (Table 1). However, in the case of BAS it was chosen to use the values obtained by the adsorption of pyridine at 250°C that are more reliable as the peak of the pyridine bound to the BAS is partly overlapping with another peak in the spectra recorded at 150°C. Nevertheless, the values of BAS are marginally dependent on the temperature of desorption of the pyridine, making the error minimal in the comparison of LAS and BAS evaluated at different temperatures.

Albeit at this stage of the research it is not possible to discriminate on which kind of acid sites the aromatics are formed, the trend is the same independent on the nature of the acid sites considered. Therefore, in general it can be concluded that the lower is the concentration, the higher the activity of the acid sites in the aromatic production. On the other hand, a high concentration of acid sites decreases their activity. It can be assumed that the formation of coke on a single catalytic site has higher probability to deactivate other acid sites that are located on its vicinity, leading to a mechanism of cross-deactivation of the sites. This mechanism can be further enhanced by the presence of paired Brønsted acid sites, which are more abundant in Al-rich zeolites, such as HZSM-5–23. According to the literature, the presence of paired acid sites can enhance the reactivity towards aromatization reactions with different feeds [34,35]. However, although beneficial for aromatic production, the presence of zoned Al sites promotes the deactivation too [36]. Furthermore, as for the production of C8 aromatics, the product distribution of the isomers gives important information about the location of the catalytic sites that are responsible for the aromatic production. Specifically, the MFI structure is well known to form preferentially p-xylene in the xylenes isomerization, due to the product and transition state selectivity [23]. On the other hand, the production of C8 is not selective towards p-xylene, for any of the catalysts investigated. Their production is summarized in Table 2, where m-xylene and p-xylene are grouped as separation with the current gas-chromatographic analysis was not possible. The values are compared with the values at the thermodynamic equilibrium at 800 K, according to the literature [37]. Even though there are differences in the C8 product distribution between different catalysts, all the relative concentrations of the isomers are close to the thermodynamic equilibrium. This evidence clearly shows how the aromatics are produced on the outer surface of the zeolite crystals, since no selectivity towards p-xylene was observed. Reasonably, all the aromatics with eight or more carbon atoms are therefore produced on the outer crystal surface of the zeolites. However, these findings are not fully conclusive, since p-xylene cannot be detected in an independent way.

3.3. *Characterization of the spent catalysts*

At the best of our knowledge, the only reported case of the spent catalyst's characterization from the aromatization of ethanol and furfural involves the TPO analysis of the HZMS-5–23 after experiments with a feed different from the current study, namely neat furfural and mixtures of furfural/ethanol and furfural/methanol [13]. Several

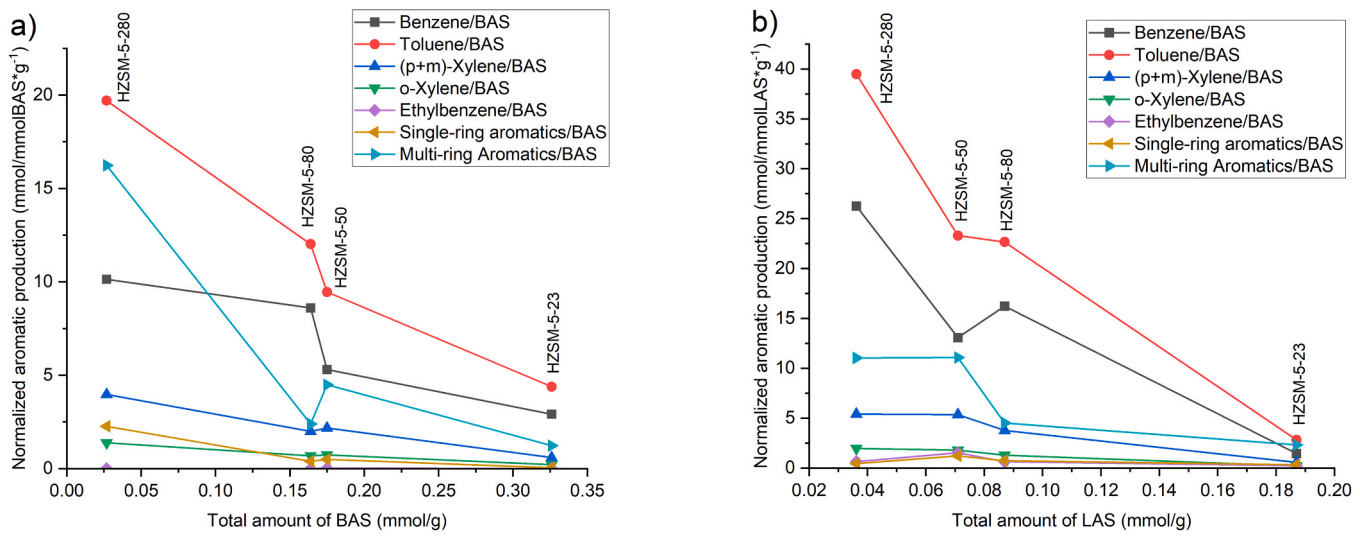

Fig. 9. Production of aromatics for a single acid site as a function of a) Brønsted acid sites concentration and b) Lewis acid sites concentration.

Table 2
Relative concentration of C8 aromatics produced by different HZSM-5 catalysts.

	Experimental values (%)				Thermodynamic limit (%)	
	HZSM-5–23	HZSM-5–50	HZSM-5–80	HZSM-5–280		
o-xylene	24.5	20.7	22.6	19.9	22	
m-xylene	67.6	61.6	66.3	56.8	46	67[a]
p-xylene					21	
ethylbenzene	7.9	17.7	11.1	23.3	16	

[a] sum of relative concentration of o-xylene and p-xylene

examples of reactions forming coke over ZSM-5 zeolites are, however, reported in the literature with similar reactions, such as the catalytic fast pyrolysis of biomass. Coke is highlighted as the main cause of catalyst deactivation, due to the formation of graphitic coke on the Brønsted acid sites [38], whereas Lewis acid sites are less affected [39]. Alcohols are less prone to form carbon deposits when compared to other oxygenated compounds, and in general a decrease of the H/C ratio of the feed enhances deactivation [40]. If the presence of alcohols generates a "hydrocarbon pool" that can lead to the formation of coke, the presence of furfural and in-situ generated furan opens further routes for the carbon deposit formation. In fact, furan can produce oxygenated polycyclic compounds, which polymerize to form larger oxygenated compounds that eventually generate coke [26,41]. Therefore, it was decided to have a more detailed analysis of the spent catalysts, by including more characterization techniques applied to the spent catalysts with different SiO_2/Al_2O_3 ratios. This strategy provides a better insight on the mechanisms of the reaction and deactivation. To this end, spent catalysts were characterized with nitrogen physisorption, TGA, elemental analysis, Raman spectroscopy and XRD.

From the TGA analysis (Table 3 and SI8) it was possible to calculate the amount of carbon deposits formed during the reaction.

The onset temperature is calculated from the intercept with the line tangent to the plateau in the weight loss before the decomposition of the carbon deposit and the line tangent to the point of the maximum slope of the curve in the range of temperature where the decomposition of the coke takes place. This value can be considered as the temperature in which the degradation by oxidation of the carbon deposit starts [42]. Another important parameter is the inflection point of the degradation curve, representing the temperature in which the rate of the carbon deposit degradation is higher. This point corresponds with the derivative of the weight loss as a function of temperature. From the results in Table 3 it can be noticed that the onset temperature is determined by the reaction conditions and not by the features of the catalyst, i. e. the SiO_2/Al_2O_3 ratio. In fact, beginning of carbon deposits degradation of the four studied catalysts spans in the range of 530°C-538°C. Similarities of the carbon deposit of the four different zeolites are confirmed by the inflection point, which differs only by 5.5°C between the four spent catalysts. This suggests that the nature of the carbon deposit formed over the zeolites with different SiO_2/Al_2O_3 ratios was the same. More carbon deposits were formed over HZSM-5–50, whereas HZSM-5–23 has a lower content of coke after aromatization. Interestingly, the trend in the coke amount on the HZSM-5–23, HZSM-5–50 and HZSM-5–80 catalysts followed the same for all the aromatics larger than benzene and toluene (Fig. 7) and the trend of benzofuran. In fact, the total production of benzofuran was 0.015 mmol, 0.148 mmol and 0.054 mmol for HZSM-5–23, HZSM-5–50 and HZSM-5–80, respectively. It can be concluded that higher production of heavy aromatics and benzofuran gave a higher coke deposition on the catalysts. Both the formation of heavy aromatics and benzofuran can be correlated to the formation of carbon deposits [43,44]. However, HZSM-5–280 catalyst represents an

Table 3
Results of TGA analysis of spent catalysts.

Catalyst	Reaction conditions	Onset temperature [°C]	Inflection point(s) [°C]	Weight loss (%)
HZSM-5–280	500°C, FFL/EtOH 1:2	535.3	587.2	9.23
HZSM-5–80	500°C, FFL/EtOH 1:2	535.6	592.6	14.02
HZSM-5–80	500°C, pure furfural	526.7	553.7	17.90
HZSM-5–80	500°C, pure ethanol	197.4 – 523.6	219.2 – 583.2	3.17
HZSM-5–80	300°C, FFL/EtOH 1:2	420.0	409.3 – 553.2	12.81
HZSM-5–80	400°C, FFL/EtOH 1:2	477.4	562.7	14.39
HZSM-5–50	500°C, FFL/EtOH 1:2	530.7	598.1	14.59
HZSM-5–23	500°C, FFL/EtOH 1:2	538.2	597.6	13.74

exception in this trend, as the amount of the carbon deposit formed on the spent catalyst is much lower when compared with the other zeolites. The much lower acidity of HZSM-5–280 makes the catalyst less active towards aromatization, causing at the same time a lower coke formation on the spent catalyst, which is anyway enough to completely stop its activity in the aromatization after 320 min of TOS. Interestingly, this catalyst has a lower BTX yield, while the formation of multi-ring aromatics is comparable with the HZSM-5–23 and HZSM-5–80 catalysts (Fig. 7). Moreover, HZSM-5–280 exhibits the highest production of benzofuran, reaching 0.290 mmol. Such a high yield of benzofuran production could explain its total deactivation towards aromatics despite a lower carbon deposit formation.

A minor effect was observed in the TGA analysis of the catalysts recovered from the two experiments using the single reactants (Fig. SI8). In terms of the onset temperature the difference between HZSM-5–80 after the experiment with the mixture of the reactants and the experiments with single reactants was only −8.9°C and −12.0°C for the experiments with neat furfural and ethanol, respectively. The inflection points were, however, different for different feeds. In particular, in the case of neat furfural, the inflection point is much lower (553.7°C), while for ethanol the main inflection point was almost at the same temperature as for the spent catalyst in the experiment using the mixture of the reactants. However, in this case other carbon deposits were present, removed at a lower temperature during TGA. Interestingly some carbon deposits were degraded at a temperature much lower than the temperature used in the catalytic experiment (500°C). This points out how the nature of this carbon deposit was different as it is more efficiently removed by the oxidative atmosphere applied under TGA analysis than under the anaerobic conditions of the catalytic experiment. Finally, the amount of carbon deposit formed when using furfural as the feed is much higher than in the case of other spent catalysts, which can be related to stronger deactivation obtained with furfural as the feed. On the other hand, the experiment with neat ethanol as the feed produced a much lower amount of the carbon deposit. To have better understanding of the nature of the carbon deposits formed depending on the composition of the feed, nitrogen physisorption and elemental analysis of the spent catalysts were also performed. The results are summarized in Table 4, where the difference in the parameters defining the morphological properties are calculated, and in Table 5 reflecting the results of the elemental analysis.

From these characterizations it can be seen how the presence of furfural under reaction conditions formed a carbon deposit that almost completely blocks the pores of the zeolite, reducing the surface area to a few tens of m^2/g. This area is generated mainly by the contribution of the external surface area, meaning that the micropores of the structure are completely obstructed. On the other hand, the experiment with neat ethanol formed a lower amount of coke, leading to a small decrease of the surface area (-78 m^2/g), without affecting the area of the mesopores. This trend resembles the one for the catalyst deactivation (Fig. 5), and confirms the hypothesis that presence of furfural is the main origin of the carbon deposit formation and catalyst deactivation. From the elemental analysis, it can be seen that a higher fraction of furfural in the feed resulted in a lower hydrogen to carbon ratio. Therefore, by increasing the fraction of furfural there is a change of the nature of the carbon deposit from aliphatic to the graphitic one [45] (Table 5). Moreover, the total fraction of hydrogen and carbon loss has a good correspondence with the weight loss in the case of the spent catalyst recovered from the experiment with neat ethanol or with the mixture of ethanol and furfural. On the other hand, in the catalyst recovered from the experiment with neat furfural, the amount of coke detected by TGA is higher than the sum of carbon and hydrogen detected in the elemental analysis. The undetected part, contributing to the excess of the mass observed by TGA, could be oxygen, indicating that the carbon deposits formed in the presence of neat furfural could be more oxygenated. To have a better insight on the carbon deposits structures, Raman spectroscopy characterizations of the spent catalysts with neat reactants and with the reaction mixture have been performed. The evaluation of the D band

Table 5
Elemental analysis of the spent HZSM-5–80 catalysts.

Feed composition	Hydrogen content (% w/w)	Carbon content (% w/w)	Sum (% w/w)	Molar ratio H/C
Furfural + ethanol 1:2	0.958	14.7	15.7	0.78
Furfural	0.601	14.7	15.3	0.49
Ethanol	0.041	2.3	2.6	1.58

Table 4
Characterization of morphology of the spent catalysts from nitrogen physisorption analysis.

Feed composition	Temperature [°C]	Surface area [m^2/g]	Difference [m^2/g]	External surface area [m^2/g]	Difference [m^2/g]	Total pore volume [m^3/g]	Micropores volume [m^3/g]	Total difference in pores volume [m^3/g]	Difference in micropores volume [m^3/g]
HZSM-5–280									
Furfural + ethanol 1:2	500	303	- 155	114	- 48	0.15	0.14	- 0.11	- 0.07
HZSM-5–80									
Furfural + ethanol 1:2	500	11	- 478	6	- 149	0.01	0.01	- 0.27	- 0.23
Furfural + ethanol 1:2	400	13	- 476	12	- 143	0.01	0.01	- 0.26	- 0.22
Furfural + ethanol 1:2	300	20	- 469	5	- 150	0.02	0.01	- 0.26	- 0.22
Furfural	500	21	- 468	4	- 151	0.02	0.01	- 0.26	- 0.22
Ethanol	500	411	- 78	167	+ 12	0.24	0.19	- 0.03	- 0.04
HZSM-5–50									
Furfural + ethanol 1:2	500	49	- 413	12	- 131	0.04	0.02	- 0.20	- 0.20
HZSM-5–23									
Furfural + ethanol 1:2	500	11	- 415	5	- 138	0.02	0.01	- 0.20	- 0.21

("defect", ~1350 cm^{-1}) and the G band ("graphite", 1580–1600 cm^{-1}), related to the ring breathing modes and sp^2 carbon atoms motion, respectively [46], provides a fingerprint of the structure of the carbon deposits (Figures are reported in SI9).

Table 6
Intensity of characteristic bands of the Raman characterization

Feed composition	D band [cm^{-1}]	Width D band [cm^{-1}]	G band [cm^{-1}]	Width G band [cm^{-1}]	Ratio intensity ID/IG
Furfural + ethanol 1:2	1378	39	1611	39[a]	0.19
Furfural	1372	39	1605	52	0.17
Ethanol	1343	40	1597	40	0.85

[a] additional peak present at 1563 cm^{-1} with width of 39 cm^{-1}.

Moreover, the samples exposed to furfural show another characteristic band at about 1200 cm^{-1}, which can be ascribed to the S band typical of the C-O-C functionality of ethers [47,48]. Summing up the Raman characterization results, the spent catalyst from the experiment using neat furfural exhibits a G band close to a band of 1606 cm^{-1}, suggesting more ordered graphitic domains, and a low ID/IG ratio which confirms the presence of a more graphitic carbon. On the other hand, ethanol produces a more disordered coke with less extended graphitic domains, which can be deduced by the location of the G band at lower wavenumber and a higher ID/IG ratio. Therefore, furfural promotes polymerization and condensation reactions, leading to graphitic coke that blocks pores and causes severe deactivation, whereas the less ordered nature of the coke formed by ethanol has a limited effect on the catalytic activity. By co-feeding furfural and ethanol, the carbon deposit has intermediate features, although the effect of furfural prevails. In fact, the ID/IG value indicates the presence of extended graphitic domain, but the strong G band shift suggests structural strain. Hence, it can be concluded that the presence of ethanol modifies coke formation pathways, reducing heavy condensation and preventing a fast deactivation as observed when furfural is the only reactant. Finally, the S band is visible only in the presence of furfural, suggesting that the resulting carbon deposit is more oxygenated than the one produced by ethanol. Oxygenated groups may decorate the edges or defects of the graphitic domains, implying that the reaction conditions favour incomplete deoxygenation of the furan rings, in line with TGA analysis. Summarizing, on one hand the presence of ethanol under reaction conditions produces a small amount of the carbon deposits with a disordered nature and smaller graphitic domains, which only partially blocks the pores of the zeolite and leads to partial deactivation of the catalyst for TOS < 320 min. On the other hand, the presence of furfural generates a higher amount of coke, more graphitic in nature, higher in oxygen content, which completely deactivates the catalyst.

As for the effect of temperature on the formation of the carbon deposits, according to Table 4, a lower temperature gives a lower decrease in the surface area and the pore volume. However, this trend is of a low magnitude (Fig. 10a).

According to TGA analysis the main difference observed for the spent catalysts from experiments at different temperatures is related more to the nature of the carbon deposits rather than its capability to block the pores. Regarding the effect of the SiO_2/Al_2O_3 ratio, the total surface area of the spent catalysts is equal for HZSM-5–80 and HZSM-5–23 catalysts, whereas HZSM-5–50 catalyst still exhibited a 49 m^2/g. HZSM-5–50 catalyst did not display a decrease in the conversion at the end of the catalytic experiment. It can be assumed that deactivation continues after TOS = 320 min while the total blockage of the micropores can be related to the conversion of ethanol and furfural, with this phenomenon not strictly related to the production of aromatics. This effect is more evident for HZSM-5–280 that displays a surface area loss of only 155 m^2/g, where due to its lower acidity the kinetics of coke formation is slower. In this case also a decrease of the conversion is not observed at the end of the catalytic experiment. However, for all cases during catalytic experiments production of aromatics stopped much earlier than the total blockage of the micropores of the zeolites.

The fresh and spent catalysts were characterized with XRD to evaluate any possible changes in the crystal structure of the zeolites after the catalytic experiments. The XRD pattern of the fresh catalysts matches the reference [49], whereas some minor changes were detected in the deactivated catalysts. This effect was evident for all the spent HZSM-5 catalysts. Here HZSM-5–80 is reported as an example, while the diffractograms of the other catalysts are reported in the supplementary information (see SI10 section). In the same way as reported by Alvarez et al. [50], the main differences occurred at about 2θ = 23°, 30° and 45°.

More specifically (Fig. 11), the two lines corresponding to the (332) at and (051) reflections at 2θ = 23.08° and 23.26° respectively, merge into a single line at 2θ = 23.16°, together with a general modification of the relative intensity of the peaks in the area between 2θ = 23° and 24°. Moreover, the doublet at 2θ of 45.053° and 45.48°, corresponding to the (1000) and (0100) reflections merged into a single reflection at 2θ of 45.265°.

According to the reference [50], these minor changes resemble a change in the cell parameters which leads the *a* and *b* vectors to become more similar in length. This feature is a clear hint of the pore filling by the coke formed during the catalytic experiment, as the modification of the cell parameters is a consequence of this phenomenon. These changes are reversible as the original structure can be restored by coke removal

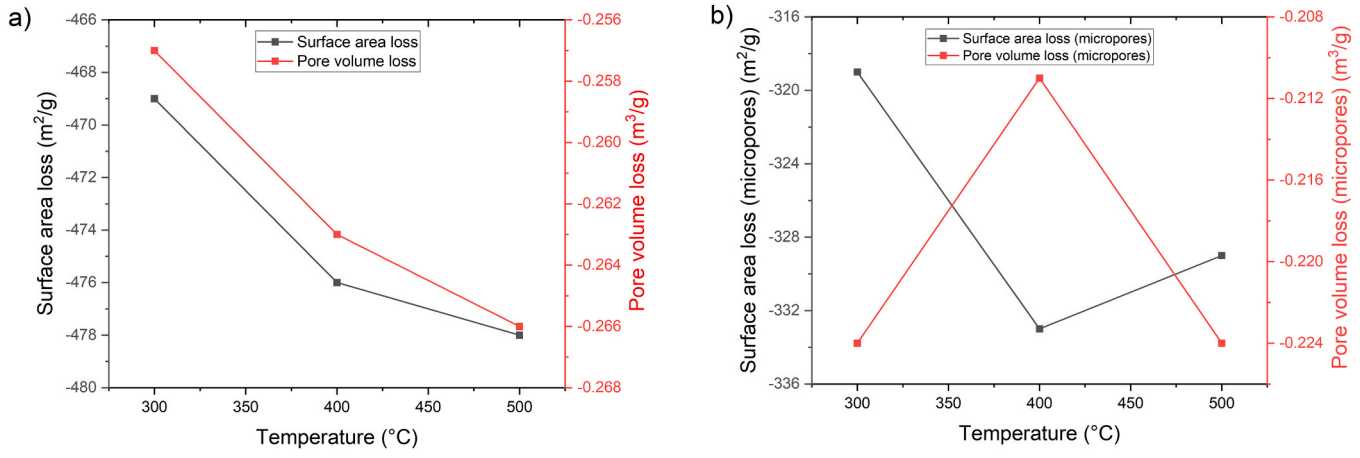

Fig. 10. Effect of the carbon deposits on the morphology of spent HZMS-5–80 catalyst. a) surface area and pore volume loss, b) loss of surface area and volume of micropores.

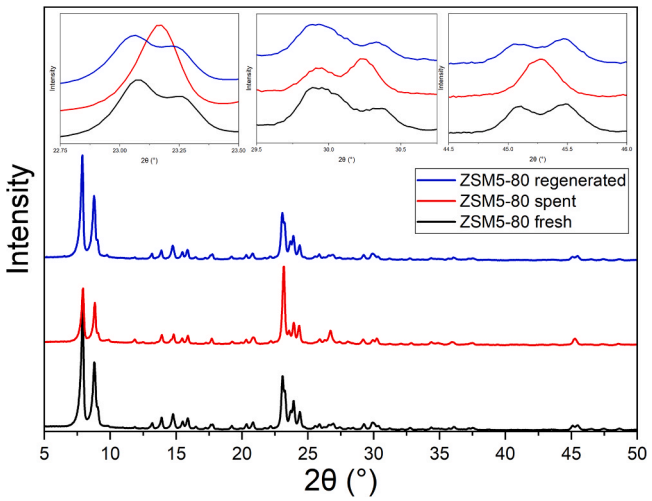

Fig. 11. XRD pattern of HZSM-5–80 catalyst. Black: fresh catalyst. Red: spent catalyst from the experiment with a feed of ethanol/furfural 2:1, T = 500°C and WHSV= 2.8 h^{-1}. Blue: catalyst regenerated upon calcination at 800°C.

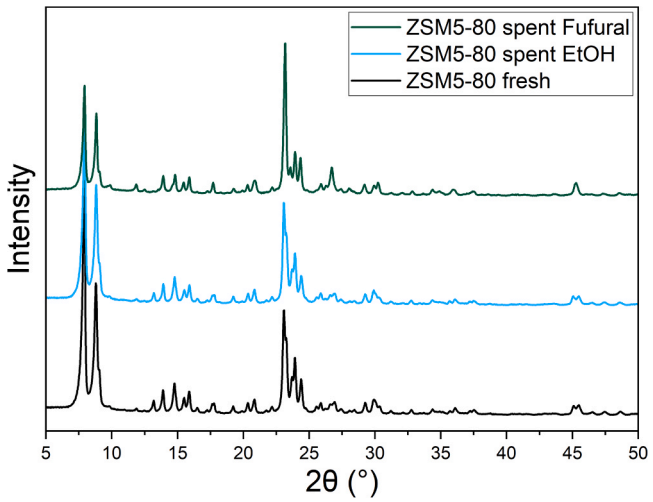

Fig. 12. XRD pattern of HZSM-5–80 from experiments with different feed. Black: fresh catalyst. Light blue: spent catalyst from the experiment with neat ethanol, T = 500°C and WHSV = 2.8 h^{-1}. Green: spent catalyst from the experiment with neat furfural, T = 500°C and WHSV = 2.8 h^{-1}.

with calcination at 800°C, as evidenced from the XRD data of the regenerated catalyst (Fig. 11). Finally, the absence of the baseline modification of the XRD diffractogram of the spent catalyst excludes the presence of an amorphous carbon phase, meaning that coke formation occurs mainly into the pores of the zeolites and only a small layer could be formed on the outer surface of the catalysts grains, which remains undetected in the XRD analysis. According to the nitrogen physisorption results, this coke formation occurs all along of catalytic experiments and can be still uncompleted after 320 min TOS, as in the case of HZSM-5–50 and HZSM-5–280. It can be concluded that the external surface of the zeolite is more active in the formation of aromatics and is easily deactivated by an outer layer of a carbon deposit at the beginning of the reaction. On the other hand, the acid sited in the micropores are more active in the decarbonylation/dehydration reactions, and their reactivity is retained until a total filling of the pores by coke. However, it cannot be excluded that aromatics are formed also in the micropores, but their diffusion outside of the pore system is not efficient and they are most likely retained in the micropores, where they act as coke precursors. Furthermore, the spent HZSM-5–80 catalysts from the experiments with neat ethanol and neat furfural were analyzed with XRD (Fig. 12), highlighting how the structural modification of the ZSM-5 lattice occurs due to the presence of furfural, whereas with neat ethanol no modifications are observed, even though a carbon deposit is present after the reaction. It can be concluded that furfural is responsible for the pore blockage by the carbon deposit, while in the presence of neat ethanol this phenomenon does not occur, allowing the aromatics formed in the micropores to back-diffuse from the pores, therefore achieving aromatics production that is more steady over time. However, the reactions involved in the presence of both ethanol and furfural are substantially different from those occurring in the case of single reactants. Hence, the nature of coke build-up in the pores can be different and ethanol can take part in this mechanism as well.

As a general observation, it can be stated that the catalytic activity in BTX formation and its deactivation are strongly affected by experimental parameters such as the reaction temperature and the feed composition, as well as by the catalyst properties per se, mainly the acid sites concentration. The feed composition and temperature are determining the pathways in the reaction network (Fig. 1), spanning from olefins production and cyclization to form aromatics, production of oxygenated compounds and related oxygen-rich coke and aromatization by the Diels-Alder mechanism. The oxygenated compounds and coke are both formed in the case of neat furfural as the feed or when using temperatures below 500°. Conversely, at 500°C the temperature is high enough to initiate the Diels-Alder reaction, leading to formation of aromatics and partially inhibiting strong deactivation imposed by furfural. While the reaction conditions are mainly affecting the pathways of the reaction network and characteristics of the carbon deposits, the materials properties are mainly determining the aromatic yield and deactivation kinetics. The main parameter influencing the catalytic behavior is the acid sites concentration, which has to be high enough for sufficient BTX production, without being too high to avoid the cross-deactivation of the catalytic sites. As for the acid sites strength, all zeolites present the same features, having mainly strong BAS and weak LAS. Consequently, current investigations do not provide a clear relationship between the acid sites strength and catalytic activity.

4. Conclusions

The production of benzene, toluene and xylenes (BTX) from renewable sources is of fundamental importance in the context of a circular and sustainable chemical industry and its independency on the fossil feedstock relying on crude oil. In this framework, BTX production from biomass-derived ethanol and furfural over HZSM-5 with varying SiO_2/Al_2O_3 ratios 23, 50, 80, 280 and Hβ with SiO_2/Al_2O_3 38 zeolite catalysts was studied as a novel route to obtain green aromatics. In the pioneering study using HZSM-5 zeolites as the catalysts, only a preliminary exploration of the reaction was reported, leaving many questions unresolved, such as the impact of the acid sites properties and concentration on the performance of the catalyst as well as the mechanism of deactivation. Starting from this, it was found that the main feature defining the performance of the catalysts is the SiO_2/Al_2O_3 ratio, that was found to be in the optimal values with the middle acidic zeolites (SiO_2/Al_2O_3 = 50 or 80). While the low aluminum containing zeolite (SiO_2/Al_2O_3 = 280) has limited acidity that results in a low yield of BTX, the zeolite exhibiting high acidity (SiO_2/Al_2O_3 = 23) was already deactivated at low TOS. In fact, high acidity results in a cross-deactivation of the acid sites, which was not observed for medium acid zeolites. However, with the reported results is not possible to distinguish whether the fast deactivation is promoted by the Brønsted or the Lewis acid sites. The largest limitation of this approach is in the catalyst deactivation, due to the formation of the carbon deposit under reaction conditions. As almost no characterization data of the spent catalysts from the aromatization of furfural and ethanol are available in the open literature, extensive characterization of the deactivated catalysts with several techniques was performed in the current work. By coupling catalytic results and characterization of the

spent catalysts it was found how deactivation occurs in two steps being mainly caused by furfural, or the in-situ produced furan. The first step is related to the formation of coke on the outer surface of the catalyst, which corresponds to the termination of the BTX production. On the other hand, the second step resembles the formation of the carbon deposit in the porous system of the zeolites, completely deactivating the catalyst. This can be detected through XRD analysis of the spent catalysts, where a minor modification of the crystal structure caused by the formation of cokes in the pores is noticed. This work shades a light on the mechanism of catalyst deactivation, together with a description of the nature and location of the acid sited that are involved in the BTX formation, that can be considered as a starting point for the design of more efficient catalysts for the production of green aromatics.

CRediT authorship contribution statement

Francesco Sandri: Writing – original draft, Methodology, Investigation. **Jennifer Cueto:** Methodology, Investigation. **Christoph Schmidt:** Investigation. **Teija Tirri:** Resources, Methodology. **Mika Lastusaari:** Methodology, Investigation. **Anssi Peuronen:** Investigation. **Pia Damlin:** Investigation. **Päivi Mäki-Arvela:** Supervision, Methodology. **Murzin Dmitry:** Writing – review & editing, Supervision, Methodology, Funding acquisition, Conceptualization. **Narendra Kumar:** Methodology. **Serrano David:** Supervision, Methodology.

Declaration of Competing Interest

The authors declare that they have no known competing financial interests or personal relationships that could have appeared to influence the work reported in this paper.

Acknowledgements

This work is financed by Business Finland, as a part of the GreenAro Project, within Neste Veturi funding scheme. This work has also received funding from the State Research Agency, MCIN/AEI /10.13039/501100011033, through the grant with reference number CEX2019-000931-M received in the 2019 call for “Severo Ochoa Centres of Excellence” and “María de Maeztu Units of Excellence” of the State Programme for Knowledge Generation and Scientific and Technological Strengthening of the R&D&I System.

Appendix A. Supporting information

Supplementary data associated with this article can be found in the online version at doi:10.1016/j.apcata.2025.120718.

Data Availability

Data will be made available on request.

References

[1] ⟨https://www.mordorintelligence.com/industry-reports/benzene-toluene-xylene-btx-market⟩.
[2] P. Khemthong, C. Yimsukanan, T. Narkkun, A. Srifa, T. Witoon, S. Pongchaiphol, S. Kiatphuengporn, K. Faungnawakij, Advances in catalytic production of value-added biochemicals and biofuels via furfural platform derived lignocellulosic biomass, Biomass Bioenergy 148 (2021) 106033, https://doi.org/10.1016/j.biombioe.2021.106033.
[3] Y. Wu, J. Yang, G. Wu, W. Gao, E.E. Silva Lora, Y.M. Isa, K.A. Subramanian, A. Kozlov, S. Zhang, Y. Huang, Benzene, toluene, and xylene (BTX) production from catalytic fast pyrolysis of biomass: a review, ACS Sustain. Chem. Eng. 11 (2023) 11700–11718, https://doi.org/10.1021/acssuschemeng.3c01202.
[4] Z. Li, Y. Jiang, Y. Li, H. Zhang, H. Li, S. Yang, Advances in Diels–Alder/aromatization of biomass furan derivatives towards renewable aromatic hydrocarbons, Catal. Sci. Technol. 12 (2022) 1902–1921, https://doi.org/10.1039/D1CY02122B.
[5] S. Zheng, Z. Zhang, S. He, H. Yang, H. Atia, A.M. Abdel-Mageed, S. Wohlrab, E. Baráth, S. Tin, H.J. Heeres, P.J. Deuss, J.G. de Vries, Benzenoid aromatics from renewable resources, Chem. Rev. 124 (2024) 10701–10876, https://doi.org/10.1021/acs.chemrev.4c00087.
[6] H.E. Hoydonckx, W.M. Van Rhijn, W. Van Rhijn, D.E. De Vos, P.A. Jacobs, Furfural and derivatives, in: Ullmann’s Encyclopedia of Industrial Chemistry, Wiley, 2007, https://doi.org/10.1002/14356007.a12_119.pub2.
[7] I. Amghizar, L.A. Vandewalle, K.M. Van Geem, G.B. Marin, New trends in olefin production, Engineering 3 (2017) 171–178, https://doi.org/10.1016/J.ENG.2017.02.006.
[8] T. Oluokun, S. Saini, A. Verma, B. Sharma, S. Konathala, A. Vorontsov, P. G. Smirniotis, J.O. Babalola, U. Kumar, Green ethylene production from bio-ethanol with acidity controlled Barium exchanged zeolite Y catalyst, Mol. Catal. 566 (2024) 114415, https://doi.org/10.1016/j.mcat.2024.114415.
[9] J. Gancedo, L. Faba, S. Ordóñez, From Biomass to green aromatics: direct upgrading of furfural–ethanol mixtures, ACS Sustain. Chem. Eng. 10 (2022) 7752–7758, https://doi.org/10.1021/acssuschemeng.2c02285.
[10] P.G. Smirniotis, E. Ruckenstein, Maximum and time stable aromatic yield in the reforming of alkylcyclopentanes over Pt/β zeolites, Catal. Lett. 25 (1994) 351–359, https://doi.org/10.1007/BF00816314.
[11] G.J.L. de Reijer, A. Schaefer, A. Hellman, P.-A. Carlsson, Catalytic conversion of furans to aromatics over ga-mfi zeotypes with varying gallium content, Ind. Eng. Chem. Res. (2025), https://doi.org/10.1021/acs.iecr.4c03465.
[12] E.A. Uslamin, N. Kosinov, G.A. Filonenko, B. Mezari, E. Pidko, E.J.M. Hensen, Co-Aromatization of furan and methanol over ZSM-5—a pathway to bio-aromatics, ACS Catal. 9 (2019) 8547–8554, https://doi.org/10.1021/acscatal.9b02259.
[13] J. Gancedo, S. Cañete, L. Faba, S. Ordoñez, Improving the stability and selectivity of furfural-to-aromatic catalytic process by co-feeding light alcohols, J. Environ. Chem. Eng. 12 (2024) 113571, https://doi.org/10.1016/j.jece.2024.113571.
[14] J. Gancedo, L. Faba, S. Ordoñez, New approaches for obtaining renewable naphthalenes by acid-catalyzed Diels-Alder additions: the role of furan-aromatic condensations, Appl. Catal. A Gen. 685 (2024) 119907, https://doi.org/10.1016/j.apcata.2024.119907.
[15] S. Kelkar, C.M. Saffron, K. Andreassi, Z. Li, A. Murkute, D.J. Miller, T.J. Pinnavaia, R.M. Kriegel, A survey of catalysts for aromatics from fast pyrolysis of biomass, Appl. Catal. B Environ. 174–175 (2015) 85–95, https://doi.org/10.1016/j.apcatb.2015.02.020.
[16] J.S. Espindola, C.J. Gilbert, O.W. Perez-Lopez, J.O. Trierweiler, G.W. Huber, Conversion of furan over gallium and zinc promoted ZSM-5: The effect of metal and acid sites, Fuel Process. Technol. 201 (2020) 106319, https://doi.org/10.1016/j.fuproc.2019.106319.
[17] E.A. Uslamin, B. Luna-Murillo, N. Kosinov, P.C.A. Bruijnincx, E.A. Pidko, B. M. Weckhuysen, E.J.M. Hensen, Gallium-promoted HZSM-5 zeolites as efficient catalysts for the aromatization of biomass-derived furans, Chem. Eng. Sci. 198 (2019) 305–316, https://doi.org/10.1016/j.ces.2018.09.023.
[18] S. Saini, T. Oluokun, B. Sharma, A. Verma, A. Vorontsov, P.G. Smirniotis, R. Singh, N. Viswanadham, U. Kumar, Cr- and Ga-modified ZSM-5 Catalyst for the production of renewable BTX from bioethanol, ChemPlusChem 89 (2024) e202300572, https://doi.org/10.1002/cplu.202300572.
[19] C.A. Emeis, Determination of integrated molar extinction coefficients for infrared absorption bands of pyridine adsorbed on solid acid catalysts, J. Catal. 141 (1993) 347–354, https://doi.org/10.1006/jcat.1993.1145.
[20] T. Degen, M. Sadki, E. Bron, U. König, G. Nénert, The HighScore suite, Powder Diffr. 29 (2014) S13–S18, https://doi.org/10.1017/S0885715614000840.
[21] S. Gates-Rector, T. Blanton, The powder diffraction file: a quality materials characterization database, Powder Diffr. 34 (2019) 352–360, https://doi.org/10.1017/S0885715619000812.
[22] R. Suerz, K. Eränen, N. Kumar, J. Wärnå, V. Russo, M. Peurla, A. Aho, D. Yu. Murzin, T. Salmi, Application of microreactor technology to dehydration of bio-ethanol, Chem. Eng. Sci. 229 (2021) 116030, https://doi.org/10.1016/j.ces.2020.116030.
[23] E.G. Derouane, Molecular shape-selective catalysis in zeolites - Selected topics, in: S. Kaliaguine, A. Mahay (Eds.), Studies in Surface Science and Catalysis, Elsevier, 1984, pp. 1–17, https://doi.org/10.1016/S0167-2991(09)60078-1.
[24] G. Catana, D. Baetens, T. Mommaerts, R.A. Schoonheydt, B.M. Weckhuysen, Relating structure and chemical composition with Lewis acidity in zeolites: a spectroscopic study with probe molecules, J. Phys. Chem. B 105 (2001) 4904–4911, https://doi.org/10.1021/jp003091v.
[25] S.R. Batool, V.L. Sushkevich, J.A. van Bokhoven, Factors affecting the generation and catalytic activity of extra-framework aluminum Lewis acid sites in aluminum-exchanged zeolites, ACS Catal. 14 (2024) 678–690, https://doi.org/10.1021/acscatal.3c04195.
[26] Y.-T. Cheng, G.W. Huber, Chemistry of furan conversion into aromatics and olefins over HZSM-5: a model biomass conversion reaction, ACS Catal. 1 (2011) 611–628, https://doi.org/10.1021/cs200103j.
[27] F.F. Madeira, N.S. Gnep, P. Magnoux, S. Maury, N. Cadran, Ethanol transformation over HFAU, HBEA and HMFI zeolites presenting similar Brønsted acidity, Appl. Catal. A Gen. 367 (2009) 39–46, https://doi.org/10.1016/j.apcata.2009.07.033.
[28] V.A. Koveza, O.V. Potapenko, A.V. Lavrenov, Catalytic conversion of ethanol to aromatic hydrocarbons in the presence of zeolite catalysts, Catal. Ind. 16 (2024) 39–57, https://doi.org/10.1134/S2070050424010033.
[29] E.G. Derouane, J.B. Nagy, P. Dejaifve, J.H.C. van Hooff, B.P. Spekman, J. C. Védrine, C. Naccache, Elucidation of the mechanism of conversion of methanol and ethanol to hydrocarbons on a new type of synthetic zeolite, J. Catal. 53 (1978) 40–55, https://doi.org/10.1016/0021-9517(78)90006-4.
[30] R. Le Van Mao, P. Levesque, G. McLaughlin, L.H. Dao, Ethylene from ethanol over zeolite catalysts, Appl. Catal. 34 (1987) 163–179, https://doi.org/10.1016/S0166-9834(00)82453-7.

[31] D. Fan, D.-J. Dai, H.-S. Wu, Ethylene formation by catalytic dehydration of ethanol with industrial considerations, Materials 6 (2013) 101–115, https://doi.org/10.3390/ma6010101.
[32] I. Takahara, M. Saito, M. Inaba, K. Murata, Dehydration of ethanol into ethylene over solid acid catalysts, Catal. Lett. 105 (2005) 249–252, https://doi.org/10.1007/s10562-005-8698-1.
[33] W.-L. Fanchiang, Y.-C. Lin, Catalytic fast pyrolysis of furfural over H-ZSM-5 and Zn/H-ZSM-5 catalysts, Appl. Catal. A Gen. 419–420 (2012) 102–110, https://doi.org/10.1016/j.apcata.2012.01.017.
[34] P. Sazama, J. Dědeček, V. Gábová, B. Wichterlová, G. Spoto, S. Bordiga, Effect of aluminium distribution in the framework of ZSM-5 on hydrocarbon transformation. Cracking of 1-butene, J. Catal. 254 (2008) 180–189, https://doi.org/10.1016/j.jcat.2007.12.005.
[35] C. Song, Y. Chu, M. Wang, H. Shi, L. Zhao, X. Guo, W. Yang, J. Shen, N. Xue, L. Peng, W. Ding, Cooperativity of adjacent Brønsted acid sites in MFI zeolite channel leads to enhanced polarization and cracking of alkanes, J. Catal. 349 (2017) 163–174, https://doi.org/10.1016/j.jcat.2016.12.024.
[36] T. Li, S.-H. Chung, S. Nastase, A. Galilea, Y. Wang, I. Mukhambetov, M. Zaarour, J. C.N. de Miguel, J. Cazemier, A. Dokania, L. Panarone, J. Gascon, L. Cavallo, J. Ruiz-Martínez, Influence of active-site proximity in zeolites on Brønsted acid-catalyzed reactions at the microscopic and mesoscopic levels, Chem. Catal. 3 (2023), https://doi.org/10.1016/j.checat.2023.100540.
[37] R.D. Chirico, W.V. Steele, Thermodynamic equilibria in xylene isomerization. 5. Xylene isomerization equilibria from thermodynamic studies and reconciliation of calculated and experimental product distributions, J. Chem. Eng. Data 42 (1997) 784–790, https://doi.org/10.1021/je970030q.
[38] E. Heracleous, E. Pachatouridou, A.M. Hernández-Giménez, H. Hernando, T. Fakin, A.L. Paioni, M. Baldus, D.P. Serrano, P.C.A. Bruijnincx, B.M. Weckhuysen, A. A. Lappas, Characterization of deactivated and regenerated zeolite ZSM-5-based catalyst extrudates used in catalytic pyrolysis of biomass, J. Catal. 380 (2019) 108–122, https://doi.org/10.1016/j.jcat.2019.10.019.
[39] A.G. Gayubo, A.T. Aguayo, A. Atutxa, R. Prieto, J. Bilbao, Role of reaction-medium water on the acidity deterioration of a HZSM-5 zeolite, Ind. Eng. Chem. Res. 43 (2004) 5042–5048, https://doi.org/10.1021/ie0306630.
[40] U.V. Mentzel, M.S. Holm, Utilization of biomass: conversion of model compounds to hydrocarbons over zeolite H-ZSM-5, Appl. Catal. A Gen. 396 (2011) 59–67, https://doi.org/10.1016/j.apcata.2011.01.040.
[41] Z. Zhou, H. Liu, X. Liu, C.-H. Chin, Oxygenated polycyclic aromatic hydrocarbons as key coke precursors in coke formation during zeolite-catalyzed furfural pyrolysis, Appl. Energy Combust. Sci. 24 (2025) 100389, https://doi.org/10.1016/j.jaecs.2025.100389.
[42] N. Saadatkhah, A. Carillo Garcia, S. Ackermann, P. Leclerc, M. Latifi, S. Samih, G. S. Patience, J. Chaouki, Experimental methods in chemical engineering: thermogravimetric analysis—TGA, Can. J. Chem. Eng. 98 (2020) 34–43, https://doi.org/10.1002/cjce.23673.
[43] Y.-T. Cheng, J. Jae, J. Shi, W. Fan, G.W. Huber, Production of renewable aromatic compounds by catalytic fast pyrolysis of lignocellulosic biomass with bifunctional Ga/ZSM-5 catalysts, Angew. Chem. Int. Ed. 51 (2012) 1387–1390, https://doi.org/10.1002/anie.201107390.
[44] J. Gancedo, L. Faba, S. Ordóñez, Benzofuran as deactivation precursor molecule: Improving the stability of acid zeolites in biomass pyrolysis by co-feeding propylene, Appl. Catal. A Gen. 611 (2021) 117980, https://doi.org/10.1016/j.apcata.2020.117980.
[45] J. Cain, A. Laskin, M.R. Kholghy, M.J. Thomson, H. Wang, Molecular characterization of organic content of soot along the centerline of a coflow diffusion flame, Phys. Chem. Chem. Phys. 16 (2014) 25862–25875, https://doi.org/10.1039/C4CP03330B.
[46] A.C. Ferrari, J. Robertson, Interpretation of Raman spectra of disordered and amorphous carbon, Phys. Rev. B 61 (2000) 14095–14107, https://doi.org/10.1103/PhysRevB.61.14095.
[47] X. Li, J. Hayashi, C.-Z. Li, FT-Raman spectroscopic study of the evolution of char structure during the pyrolysis of a Victorian brown coal, Fuel 85 (2006) 1700–1707, https://doi.org/10.1016/j.fuel.2006.03.008.
[48] Q. Xu, Z. Liu, H. Jiang, Q. Zhang, C. Zan, D. Ma, L. Shi, Chemical-structural properties of the coke produced by low temperature oxidation reactions during crude oil in-situ combustion, Fuel 207 (2017) 179–188, https://doi.org/10.1016/j.fuel.2017.06.026.
[49] M. Inui, T. Ikeda, T. Suzuki, K. Sugita, F. Mizukami, Quantitative analysis of structural defect in silicalite by Rietveld refinements using X-ray powder diffraction and 29Si MAS NMR, Bull. Chem. Soc. Jpn. 82 (2009) 1160–1169, https://doi.org/10.1246/bcsj.82.1160.
[50] A.G. Alvarez, H. Viturro, R.D. Bonetto, Structural changes on deactivation of ZSM-5. A study by X-ray powder diffraction, Mater. Chem. Phys. 32 (1992) 135–140, https://doi.org/10.1016/0254-0584(92)90269-E.